

Human–Machine Shared Control for Path Following Considering Driver Fatigue Characteristics

Zhenwu Fang¹, Graduate Student Member, IEEE, Jinxiang Wang², Member, IEEE, Zejiang Wang, Jinxin Chen³, Guodong Yin⁴, Senior Member, IEEE, and Hui Zhang⁵, Senior Member, IEEE

Abstract—Fatigue driving has been regarded as one of the most important factors that cause traffic accidents. This paper proposes a robust human-machine shared control strategy to improve the vehicle performance for different driver fatigue states. Firstly, the time-varying driver steering model is proposed to address the model mismatch caused by fatigue driving. And the driver fatigue evaluation system is established based on facial features to quantify driver fatigue levels. Based on the quantified fatigue levels, a novel strategy for allocating authorities of the driver and controller is developed for building the driver-vehicle interaction system. Then, to weaken the influence of parameter perturbations caused by the time-varying driver states, we design a fatigue-based shared controller through state feedback. The actuator saturation and system constraints are considered in the controller design through the robust set-invariance property to improve vehicle safety and driving comfort. The driver-in-the-loop platform is conducted to validate the effectiveness of the proposed shared steering controller. The experimental results show that the proposed strategy can adaptively optimize the human-machine authorities according to fatigue states and comprehensively improve vehicle performance.

Index Terms—Human–machine shared control, driver model, fatigue driving, control authority.

I. INTRODUCTION

WITH the rapid development of mobile communication technology, artificial intelligence, and advanced sensors, autonomous driving technology has made a great process [1]. Nevertheless, it is challenging that fully autonomous driving technology is widely applied in commercial vehicles due to complex transportation environments, imperfect road

infrastructure, and legal issues [2], [3]. Advanced driving assistance systems (ADASs) will be still the main technology to develop intelligent vehicles in the future, which can improve driving safety and reduce drivers' workload by take-over mechanism. However, the assistance strategy leads to an uncertain take-over time, which may cause a risk of vehicle instability during the control transfer process [4]. Therefore, the human-machine shared control technology was introduced to ensure that the driver remained consistently engaged in the control loop [5], [6].

The steering assistance system has been regarded as one of the most important technologies in human-machine shared control to improve vehicle performance [7], [8]. Ahmadian et al. [9] proposed a hierarchical control framework to assist the driver by coordinating active front steering and direct yaw moment control. In [10] and [11], Ercan et al. designed a driver-vehicle coupled steering model and optimized assistance torque based on the model predictive control method. Chen et al. [12] proposed a driver-assistance lateral motion control method considering yaw moment variation to prevent lane departure. In terms of the vehicle stability control under extreme conditions, Li et al. [13] presented an integrated longitudinal and lateral vehicle stability controller with real-time envelope control regions to assist a driver. To further achieve the personalized assistance driving, driver models were introduced into the design of the assistance controller [14], [15], [16]. Wang et al. [17] proposed a shared controller based on a two-point preview driver model to reduce the physical workload of the driver. In fact, the driver's state may greatly vary due to the external factors [6], resulting in uncertainties of human-machine interaction. In the above studies, this was not considered in the design of the controller.

To realize the adaptive interaction between the driver and the controller, the concept of control authority allocation is introduced into the shared control system. Here, the control authority means the intervention level of a controller and a driver when they manipulate the vehicle simultaneously. One of the factors affecting human-machine interaction is the driver's trust in the shared steering system [18]. Some researchers tried to coordinate the authorities between the driver and controller by evaluating the driver's trust status to improve the cooperation level. The adaptive-trust authority allocation model was proposed to assist a driver efficiently [19], [20], [21]. Shi et al. [22] designed a parallel human-machine cooperation framework by analyzing the

Manuscript received 27 September 2022; revised 5 April 2023 and 30 October 2023; accepted 16 December 2023. This work was supported in part by the National Natural Science Foundation of China under Grant 52072073, Grant 52372410, and Grant 52025121; and in part by the Postgraduate Research and Practice Innovation Program of Jiangsu Province under Grant KYCX22_0198. The work of Zhenwu Fang was supported by the China Scholarship Council, during the visit of the National University of Singapore, under Grant 202306090103. The Associate Editor for this article was C. Hu. (Corresponding author: Jinxiang Wang.)

Zhenwu Fang, Jinxiang Wang, and Guodong Yin are with the School of Mechanical Engineering, Southeast University, Nanjing 211189, China (e-mail: mechinefang@gmail.com; wangjx@seu.edu.cn; ygd@seu.edu.cn).

Zejiang Wang is with the Oak Ridge National Laboratory, Oak Ridge, TN 37932 USA (e-mail: wangz2@ornl.gov).

Jinxin Chen was with the School of Mechanical Engineering, Southeast University, Nanjing 211189, China. He is now with SAIC Volkswagen Automotive Company Ltd., Shanghai 201805, China (e-mail: 220200334@seu.edu.cn).

Hui Zhang is with the School of Transportation Science and Engineering, Beihang University, Beijing 100191, China (e-mail: hui Zhang285@gmail.com).

Digital Object Identifier 10.1109/TITS.2023.3347439

driver's attitude to the machine. In fact, the human-machine interaction is also influenced by driver's states. The steering assistance system should be given a higher control authority for improving driving safety if the driver is in an abnormal state (fatigued, distracted, etc.) [23]. To address lane departure caused by distraction behaviors (smoking, calling, yawning, and drowsiness), the driving style (DS) was quantified and introduced into lateral motion control in [24]. Nguyen et al. [25], [26] designed a U-shape authority function to assist a driver under different activity levels. Particularly, a dynamic load allocation approach based on driver workload was designed to resolve human-machine conflicts and ease the driver's burden [27].

The above studies designed specific authority strategies to coordinate the interaction between the driver and the controller, which improved driving comfort and safety. Nonetheless, few existing studies so far considered varying driver fatigue states in the design of the control authority allocation strategy. Fatigue driving may cause driver misoperation, which significantly influences road safety [28], [29]. The driver's assistance requirements are different when he/she is in the different fatigued states. When the driver is fatigued, from the perspective of vehicle safety, the human-machine control system needs to weaken the driver's authority and increase the controller's assistance level. On the contrary, when the driver is awake, the driver can obtain a relatively high authority level to satisfy the individual's driving intention.

Currently, most studies of fatigue driving focused more attention on fatigue detection. Facial expressions have been considered as one of the most effective fatigue features [30], [31]. Meanwhile, the application of deep learning technology has further promoted the development of fatigue detection [32], [33], [34]. The methods proposed in these studies focus on the detection of driver fatigue (only define two states, i.e., 0 for sleepy and 1 for awake), which can not feature the driver fatigue state by different levels. To better describe the driver fatigue characteristics, Li et al. [35], [36] adopted the approximate entropy method based on the steering wheel angle and yaw angle to detect different driver fatigue levels. The steering wheel angle may be affected by many factors such as driving habits and styles, which reduces the accuracy of fatigue recognition. From the viewpoint of practical application, Liu et al. [37] established a driver fatigue fuzzy inference framework based on facial features to determine the three levels of driver fatigue. The above research mainly focuses on identifying driver fatigue, but how the steering assistance system intervenes in shared control when the driver is in a different fatigue state has not been discussed. If the intervention control of the steering assistance system can be adaptively adjusted according to quantified fatigue levels, the road safety will be greatly improved. Hence, we pay more attention to how to allocate reasonable human-machine authority levels by evaluating the fatigue state.

Time-varying driver fatigue state and authority levels may increase the nonlinearities and uncertainties of the driver-vehicle system. Takagi-Sugeno (T-S) fuzzy robust control method has been applied to the shared steering control to deal with the varying vehicle speed and authority level [25], [38].

Existing shared control studies have rarely characterized the varying driver fatigue states by T-S fuzzy modeling methods. In this paper, the driving performance under different fatigue levels is guaranteed via a T-S fuzzy robust shared controller. The main contributions of this paper can be summarized as follows:

- 1) The time-varying fatigue state may lead to driver model mismatch and even the failure of the assistance controller. This is not studied in the existing shared steering control studies. Therefore, the driver fatigue evaluation model is proposed to quantify fatigue levels. Furthermore, the driver steering model with time-varying fatigue characteristics is established based on the recursive least squares (RLS) method.
- 2) To weaken the abnormal behavior caused by fatigue driving, we introduce a control authority factor based on the driver fatigue evaluation model, which allocates control authority between two players and optimizes the steering compensation of the assistance controller.
- 3) Through using the dynamic parallel distributed compensation method, we develop the robust H_∞ shared controller for human-machine interaction to deal with system uncertainties caused by the varying fatigue characteristics and dynamic control authorities. Besides, constraints of human-machine interaction system are introduced to improve the vehicle safety.

The rest of this paper is as follows. In Section II, the time-varying driver model and driver fatigue evaluation model are established. Next, Section III presents the control design of the human-machine shared steering system considering fatigue characteristics. Section IV validates the performance of the shared steering system via the driving simulator. The final section provides a recapitulation of contributions and offers insights into future research directions.

II. MODELING OF DRIVER STEERING BEHAVIOR AND DRIVER FATIGUE EVALUATION

The driver fatigue characteristics are shown in the steering behavior and physiological features. To better describe driver steering behavior under different fatigue states, this section aims to establish a time-varying driver steering model and evaluate driver fatigue state through facial physiological features. Further, the relationship between the time-varying driver characteristic parameters and fatigue state is analyzed.

A. Time-Varying Driver Steering Model

Regarding the tracking of curved paths, multiple research investigations have showcased that a driver's anticipatory actions can be represented by observing a pair of specific visual points [39], [40]. These points are characterized by their respective distances from the vehicle's center of gravity (CG) and are denoted as preview distances l_n and l_{far} . Based on the preview information, two virtual angles θ_f and θ_n are derived as:

$$\theta_n = \frac{yL}{l_n} + \varphi_L \quad (1-1)$$

$$\theta_f = l_{far} \rho_r \quad (1-2)$$

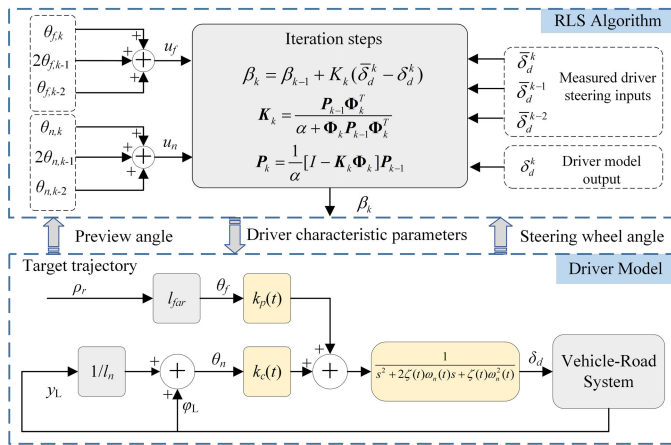


Fig. 1. Structure of time-varying driver steering model.

where $l_n = 0.4l_{far}$. l_{far} can be approximated as $v_x t_p$. t_p is driver's preview time and v_x is the vehicle speed. y_L represents the lateral deviation at the driver's preview point. φ_L denotes the heading deviation. Derived from the two virtual angles, the driver determines the steering wheel angle δ_d via the neuromuscular system [40]. This system can be modeled as a second-order approximation, demonstrated as follows:

$$\delta_d(s) = \frac{k_p(t)\theta_f(s) - k_c(t)\theta_n(s)}{s^2 + 2\zeta(t)w_n(t)s + w_n^2(t)} \quad (2)$$

where s is the Laplacian. The feedforward gain, denoted as $k_p(t)$, symbolizes the driver's predictive ability for imminent traffic conditions. In contrast, the feedback gain, labeled as $k_c(t)$, serves as the human's corrective measure to address tracking deviations. $\zeta(t)$ is the neuromuscular system damping, which reflects how often the driver adjusts the steering wheel. $w_n(t)$ is defined as the natural frequency of the neuromuscular system used to describe the driver's response time. The variations in these parameters are associated with the driver's state. Distinct levels of fatigue induce alterations in the driver's responses and steering actions while executing the driving task. To ensure the modeling accuracy under different driver fatigue states, the driver characteristic parameters $k_p(t)$, $k_c(t)$, $\zeta(t)$, and $w_n(t)$ need to be updated online based on RLS algorithm, as shown in Fig. 1. The driver model (2) is firstly transformed into the standard least squares regression model through bilinear transformation, as follows:

$$\delta_d^k = \Phi_k \beta_{k-1}^T \quad (3)$$

where δ_d^k is the estimation of the driver's steering wheel angle at time k . $\Phi_k = [-\delta_d^{k-1} \quad -\delta_d^{k-2} \quad u_f \quad u_n]$ is the measurement input of the RLS algorithm. δ_d^{k-1} is the measured driver's steering wheel angle. $\beta_{k-1} = [b_1 \quad b_2 \quad b_3 \quad b_4]$ is the identified parameter vector with driver characteristic parameters. Note that u_f , u_n , and β_k are given in Appendix A.

The forgetting factor α is introduced into the cost function of the RLS algorithm for its good convergence performance. Besides, we use the window function with a finite component N . Therefore, the performance indicator function in each time

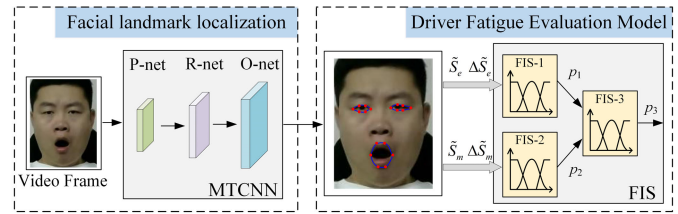


Fig. 2. Driver fatigue evaluation system.

window can be expressed as follows.

$$J(\beta_k) = \sum_{i=1}^{i=N} \alpha^{N-i} |\delta_d^k - \delta_d^k|^2 \quad (4)$$

The time-varying driver characteristic parameters can be updated by minimizing the cost function $J(\beta_k)$ as follows:

$$\beta_k = \beta_{k-1} + K_k (\delta_d^k - \delta_d^k) \quad (5-1)$$

$$K_k = \frac{P_{k-1} \Phi_k^T}{\alpha + \Phi_k P_{k-1} \Phi_k^T} \quad (5-2)$$

$$P_k = \frac{1}{\alpha} [I - K_k \Phi_k] P_{k-1} \quad (5-3)$$

where the initial value of the covariance matrix P_0 is set as σI ($\sigma \gg 0$). The initial value of β_0 is set as 0 . The forgetting factor α is selected as 0.98 to prevent data saturation. Then, the time-varying driver characteristic parameters $k_p(t)$, $k_c(t)$, $\zeta(t)$, and $w_n(t)$ can be obtained by solving the mathematical relationship between a_i ($i = 0, 1, 2$) and β_k in Appendix A.

B. Driver Fatigue Evaluation Model

Driver fatigue is one of the important factors affecting the safety of co-driving vehicles, which is usually induced by long-time driving, sleep, inattention, and other factors [28]. Long-time driving and lack of sleep are quite common fatigue-inducing factors. In addition, many studies have shown that drivers usually have obvious symptoms such as blinking and yawning after driving for a long time or lack of sleep [28], [33]. Therefore, this section designs a driver fatigue evaluation system based on facial features, as shown in Fig. 2. The experimental samples are marked based on the facial video expert evaluation method [35].

The multi-task convolutional neural network (MTCNN) including P-net, R-net, and O-Net is used to locate facial landmarks in the driver fatigue evaluation system. This approach has been widely applied in the face detection field due to its real-time accuracy. In previous studies [41], [42], five marker points were used to localize the eyes and mouth. Then, these marker points form a central rectangle to determine the closeness of the feature region, which can be used to detect fatigue. But it was difficult to quantify different levels of driver fatigue. Therefore, in order to accurately calculate the opening degree in the feature regions, we improve the MTCNN structure to obtain 18 feature points of facial regions, as shown in Fig. 2. The degree of opening of eyes and mouth are extracted as key fatigue features to develop the parallel fuzzy inference system (FIS). The first-level FIS consists of

FIS-1 and FIS-2. FIS-1 and FIS-2 are designed to evaluate eye fatigue level p_1 and mouth fatigue level p_2 , respectively. FIS-3 is the second-level FIS to evaluate the driver fatigue level p_3 based on outputs of the first-level FIS.

A third-order-polynomial curve is used to fit the upper and lower contours of the eyes and mouth regions, which can be expressed as follows:

$$y_r^{cur} = a_{r,0}^{cur} + a_{r,1}^{cur} x + a_{r,2}^{cur} x^2 + a_{r,3}^{cur} x^3 \quad (6)$$

where $r \in \{le, re, m\}$ represent the regions of the left eye, right eye, and mouth, respectively. $cur \in \{up, low\}$ represent the upper and lower contours of the feature regions, respectively. $a_{r,i}^{cur}$ ($i = 0, 1, 2, 3$) is the face contour coefficient. (x, y_r^{cur}) is the pixel coordinate of the facial key feature point. The face contour coefficient $a_{r,i}^{cur}$ can be obtained by fitting the pixel points of facial feature regions. Then, two quantitative indices including feature region area and its change are proposed to evaluate the eyes fatigue and mouth fatigue, denoted as S_r and ΔS_r , respectively:

$$S_r = \int_{x_r^{sp}}^{x_r^{ep}} y_r^{up}(x) - y_r^{low}(x) dx \quad (7-1)$$

$$\Delta S_r = S_r(t+1) - S_r(t) \quad (7-2)$$

where x_r^{sp} and x_r^{ep} represent the start and end points of the feature curve, respectively. S_r and ΔS_r are used to represent the driver's current state and the changing trend of the driver's state, respectively. Due to the significant differences in facial features of different drivers, the relative values of S_r and ΔS_r are used as inputs of the driver fatigue evaluation model as follows:

$$\tilde{S}_r = \sum \frac{S_r}{f_{ra} S_r^{max}} \quad (8-1)$$

$$\Delta \tilde{S}_r = \sum \frac{\Delta S_r}{f_{ra} \Delta S_r^{max}} \quad (8-2)$$

where S_r^{max} and ΔS_r^{max} represent the maximum value of the feature region openness. f_{ra} is the number of frames. Note that the average value of \tilde{S}_{le} and \tilde{S}_{re} is used as the feature of eye fatigue, defined as \tilde{S}_e .

The linguistic set of inputs for FIS is defined as {L,M,H}. The linguistic set of outputs for FIS is defined as {ND,MF,SF}. \tilde{S}_e and $\Delta \tilde{S}_e$ are fed to the FIS-1 to evaluate eyes fatigue level p_1 . L, M, and H represent the closed, half-open, and open states of the eyes in the FIS-1, respectively. Meanwhile, the change rate $\Delta \tilde{S}_e$ of facial regions from slow to fast is also defined as L, M, and H. The linguistic set of the output p_1 for FIS-1 is described by normal driving (ND), medium fatigue (MF), and severe fatigue (SF). The fuzzy rules for FIS-1 are shown in Table I.

When \tilde{S}_e is in the closed (L) state, the driver's eye features are considered as fatigue symptoms. At this time, $\Delta \tilde{S}_e$ is in the L or M state, which indicates that the change of the feature region is small and has little influence on the current fatigue state. Accordingly, the eye fatigue state is set as severe fatigue (SF). However, if $\Delta \tilde{S}_e$ is in the H state, it will mean that the driver has a tendency to get rid of the severe fatigue state. The eye fatigue state is set as medium fatigue (MF) state.

TABLE I
FUZZY RULES OF THE FIS-1

$\tilde{S}_e \backslash \Delta \tilde{S}_e$	L	M	H
L	SF	SF	MF
M	MF	MF	MF
H	ND	ND	MF

TABLE II
FUZZY RULES OF THE FIS-3

$p_1 \backslash p_2$	L	M	H
L	SF	SF	SF
M	MF	MF	MF
H	SF	MF	ND

When \tilde{S}_e is in the half-open (M) state, no matter $\Delta \tilde{S}_e$ belongs to the L, M, or H state, the eye states are set as the medium fatigue (MF) state. The design aims to achieve the smooth transition from the normal driving to the severe fatigue driving states.

When \tilde{S}_e is in the open (H) state and $\Delta \tilde{S}_e$ belongs to the L or M state, the driver is able to maintain a normal driving (ND) state. However, if $\Delta \tilde{S}_e$ is in the H state, it will mean that the driver has a tendency to become slightly fatigued. The eye fatigue state is set as medium fatigue (MF) state.

\tilde{S}_m and $\Delta \tilde{S}_m$ are fed to the FIS-2 to evaluate mouth fatigue level p_2 . The linguistic set of inputs for FIS-2 is defined as the open (L), half-open (M), and closed states (H) of the mouth, respectively. Meanwhile, the change rate $\Delta \tilde{S}_m$ of facial regions from slow to fast is also defined as L, M, and H. The linguistic set of the output p_2 for FIS-2 is described by a linguistic set of normal driving (ND), medium fatigue (MF), and severe fatigue (SF). Similar to the rule design of FIS-1, the fuzzy rules are used to describe the mouth fatigue states.

Then, p_1 and p_2 are used as the inputs of FIS-3 to evaluate the driver fatigue level p_3 . The linguistic set of inputs for FIS-3 is defined as the severe fatigue (L), medium fatigue (M), and normal states (H) of facial features, respectively. The linguistic set of the output p_3 for FIS-3 is described by normal driving (ND), medium fatigue (MF), and severe fatigue (SF). Eye fatigue level is the most important index representing fatigue states. Accordingly, when p_1 is in the L or M state, no matter p_2 belongs to L, M, or H states, the driver's fatigue level p_3 is set as the severe fatigue (SF) or medium fatigue (MF) states, respectively. However, when p_1 is in the H state, p_2 will determine the driver fatigue level p_3 . For example, when p_2 is in the L state, the driver fatigue level p_3 is set as SF. The fuzzy rules for FIS-3 are shown in Table II.

The gaussian and trapezoid functions are selected as the membership function of FIS. The trapezoid function is used as the boundary of FIS to distinguish the normal and severe fatigue states. Drivers with a medium fatigue state are easily influenced by the external environment [28], [29], [43]. For instance, a driver may enter into a severe fatigue state due to a long-term driving task, or may return to a normal state due

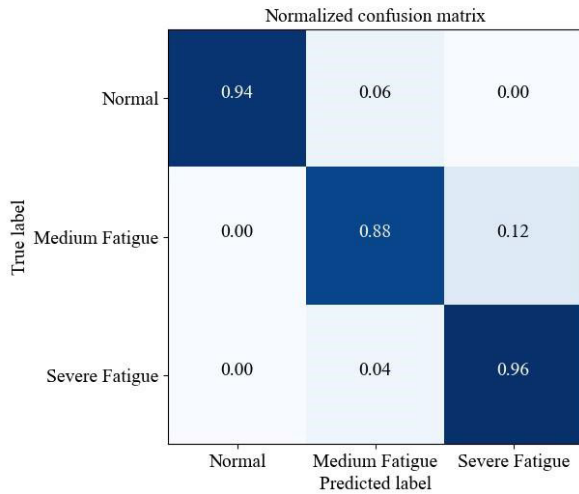


Fig. 3. Confusion matrix for three-level fatigue evaluation under testing set.

TABLE III
DRIVER FATIGUE LEVEL EVALUATION CRITERIA

Fatigue state	Features
Normal	Eyes open widely and blink quickly and eyeballs move actively. The head stays upright, and facial expressions are rich. Attentive to the environment.
Medium fatigue	Eyes tend to close, blink slowly with less eyeball activity. Drivers make gestures like shaking head, winking, swallowing, and yawning. Attention to the outside world decreases.
Severe fatigue	Eyes close further with eyelids becoming heavier. Eyes are closing for a longer time. Drivers may nap, nod their heads, and then lose the ability to drive.

to psychological stress. Hence, to ensure a smoother fatigue assessment, a gaussian function is applied for the medium fatigue state. It should be noted that the evaluation thresholds for the three fatigue levels are tuned by experimental samples.

To validate the effectiveness of the driver fatigue recognition, we recruited 9 male drivers and 6 female drivers, aged between 27 and 35 years old. Each driver had more than 5 years of driving experience. Each driver drove continuously for 1 hour in an urban scenario. Before such testing, a fatigue test needed to be completed. The detailed fatigue test can be found in Section II-C. Based on collected driver facial data, we manually defined fatigue levels for each image according to [35] and [36], as shown in Table III. Finally, 13500 labeled facial images were obtained.

The sample labels are divided randomly into 70% training set and 30% testing set. The confusion matrix for three-level fatigue evaluation under the testing set is shown in Fig. 3. It can be found that the average accuracy of the fatigue classification is over 92.7%, which indicates that the driver fatigue evaluation model is effective. In particular, the proposed fatigue evaluation method has higher identification accuracy for severe fatigue, up to 96%.

C. Driver Characteristic Parameters Boundaries Under Different Fatigue Levels

We performed U-shape road steering experiments with the radius of 75 m, 90 m, and 100 m while traveling at a constant

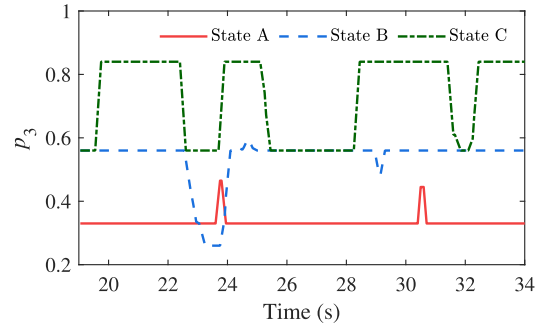


Fig. 4. Fatigue level under three different fatigue state.

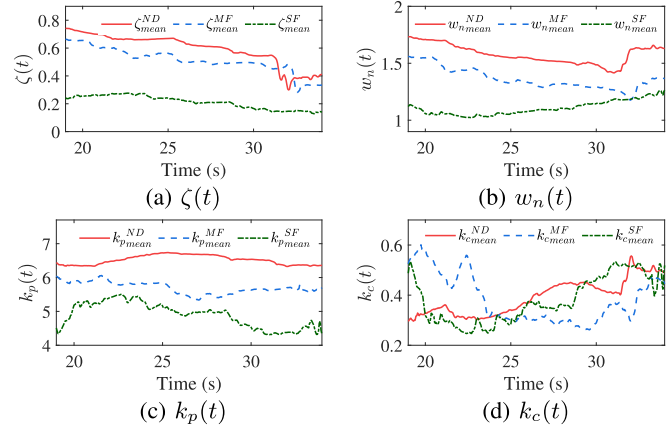


Fig. 5. Identification results of driver characteristic parameters under different fatigue levels. V_{mean}^l is the mean value of the identification parameter $V(t)$. $V \in \{\zeta, w_n, k_p, k_c\}$. $l \in \{ND, MF, SF\}$.

longitudinal speed of 20 m/s. The time-varying driver characteristic parameters of the model (2) were estimated recursively at 20 Hz using the RLS algorithm discussed. We invited fifteen drivers with different fatigue levels to participate in the experiment. All participants were experienced drivers with over five-year driving licenses and proficient in the operation of the driving simulator.

The driving time and sleep time affect the driver's fatigue states [44]. Referring to [32] and [45], the driver's fatigue states are denoted as State A, State B, and C by different driving time and sleep time, respectively. Drivers in State A perform a 20-minute urban scenario based on the driving simulator with the normal sleep time as usual. Drivers in State B perform a 60-minute urban scenario with the sleep time less than 3 hours than usual. Drivers in State C perform a 120-minute urban scenario with the sleep time less than 5 hours than usual. Drivers in States B and C have frequent features of blinking and yawning during driving tasks. Especially, the fatigue symptoms of State C are the most obvious. Therefore, States A, B, and C are denoted as normal driving, medium fatigue driving, and severe fatigue driving, respectively. Fig. 4 shows the driver fatigue levels of the States A, B, and C. It can be found that the evaluation results can accurately describe the driver's fatigue states.

The mean values of characteristic parameters of fifteen drivers are used to analyze the relationship with the fatigue level, as shown in Fig. 5. As the driver fatigue level

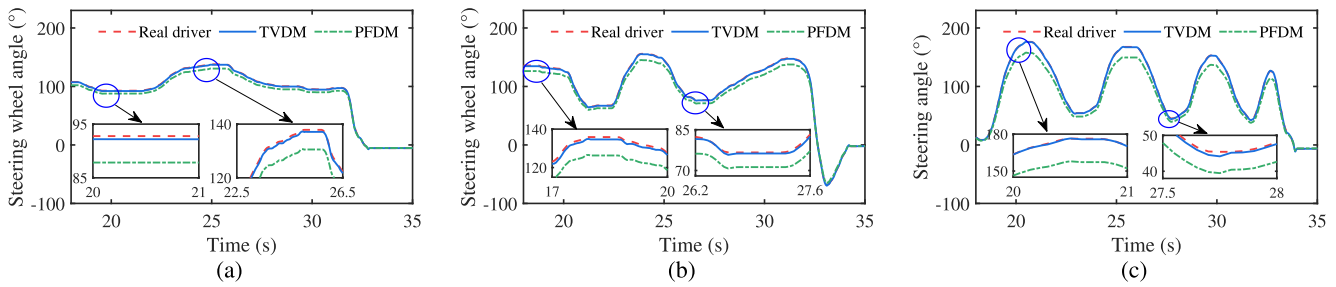


Fig. 6. Comparison between driver model and real steering behavior: (a) State A; (b) State B; (c) State C.

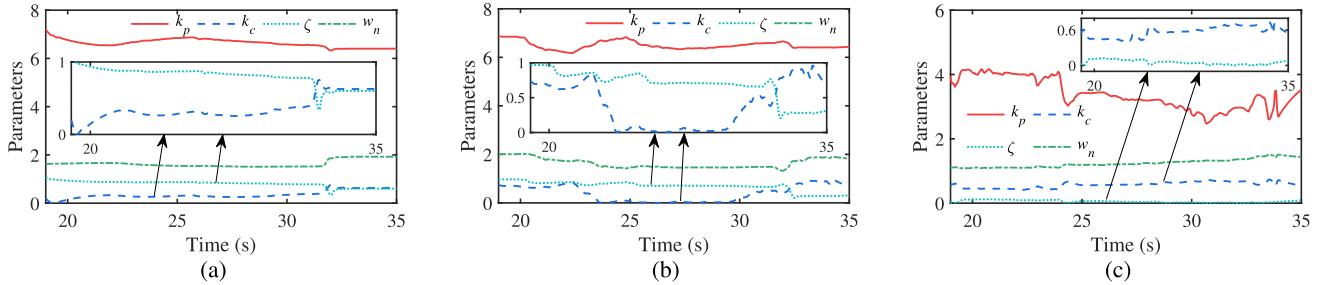


Fig. 7. Parameter identification results of a driver under different fatigue states: (a) State A; (b) State B; (c) State C.

p_3 increases, the value of $\zeta(t)$ becomes smaller, which indicates that the driver is frequently correcting the steering wheel. $w_n(t)$ represents the nature frequency of the proposed driver model, which is inversely proportional to driver's response time. As the driver fatigue level increases, the value of $w_n(t)$ becomes progressively smaller, which means that the driver's response time increases. $k_p(t)$ represents the driver's ability to perceive road curvature information. It would decrease with an increase of fatigue level. $k_c(t)$ represents the driver's ability to track the desired path. It can be found that $k_c(t)$ oscillates significantly with the increase of fatigue level, which indicates that the driver's maneuvering ability gets worse. Through a large amount of test data of fifteen drivers, the parameter boundaries for different fatigue states are given as shown in Table IV for the design of the controller.

To validate the effectiveness of time-varying driver model (TVDM), the parameter-fixed driver model (PFDM) is used as the benchmark. The real steering behavior of the driver is also given in Fig. 6. The fitting accuracy of PFDM is lower than that of TVDM in steering behavior. Especially, the steering error of PFDM has exceeded 15° under States B and C. In contrast, the fitting goodness of TVDM has reached more than 98% under different fatigue states. Fig. 7 shows the parameters identification results of the time-varying driver model. It can be found that there is a large perturbation in the driver characteristic parameters during the driving task. Meanwhile, the identification results are consistent with our parameter boundaries (seen in Table IV) under different fatigue states.

III. FATIGUE-BASED HUMAN-MACHINE SHARED SYSTEM DESIGN

A. Control Framework of Shared Steering System

The driver fatigue can lead to time-varying driver characteristics and abnormal behavior, which may cause

TABLE IV

BOUNDARIES OF DRIVER FATIGUE CHARACTERISTIC PARAMETERS

Boundaries	Fatigue State	k_p	k_c	ζ	w_n
Min	Normal	5.5	0	0.5	1.6
Max	Normal	7.5	1	1	2.4
Min	Medium	4	0	0.3	1.2
Max	Medium	7	1	0.8	2
Min	Severe	2.5	0	0.05	0.8
Max	Severe	5.5	1	0.4	1.4

human-machine conflicts and vehicle instability. To weaken the uncertainties caused by fatigue driving, we propose a control framework of shared steering system considering driver's fatigue characteristics, as shown in Fig. 8.

In the control framework, the driver's facial features are fed into the driver fatigue evaluation model (DFEM) to obtain the fatigue level. And the driver's fatigue characteristic parameters are identified in real-time. Further, the boundaries between fatigue characteristic parameters and fatigue levels are determined by analysis of test data. This work has been completed in Section II.

The fatigue level obtained from DFEM is used as the input of the authority allocation strategy to evaluate the control authority levels of the driver and controller, which aims to weaken the abnormal behavior caused by fatigue driving. In addition, the traditional driver-vehicle model used for control does not consider the driver fatigue characteristics and human-machine authority interaction, which may cause the controller failure. To this end, through using the dynamic parallel distributed compensation method, the parallel robust H_∞ shared controller considering the fatigue characteristics and authority level for human-machine interaction is designed in Section III. Distributed sub-controllers are designed based on parameter boundaries of different fatigue characteristics,

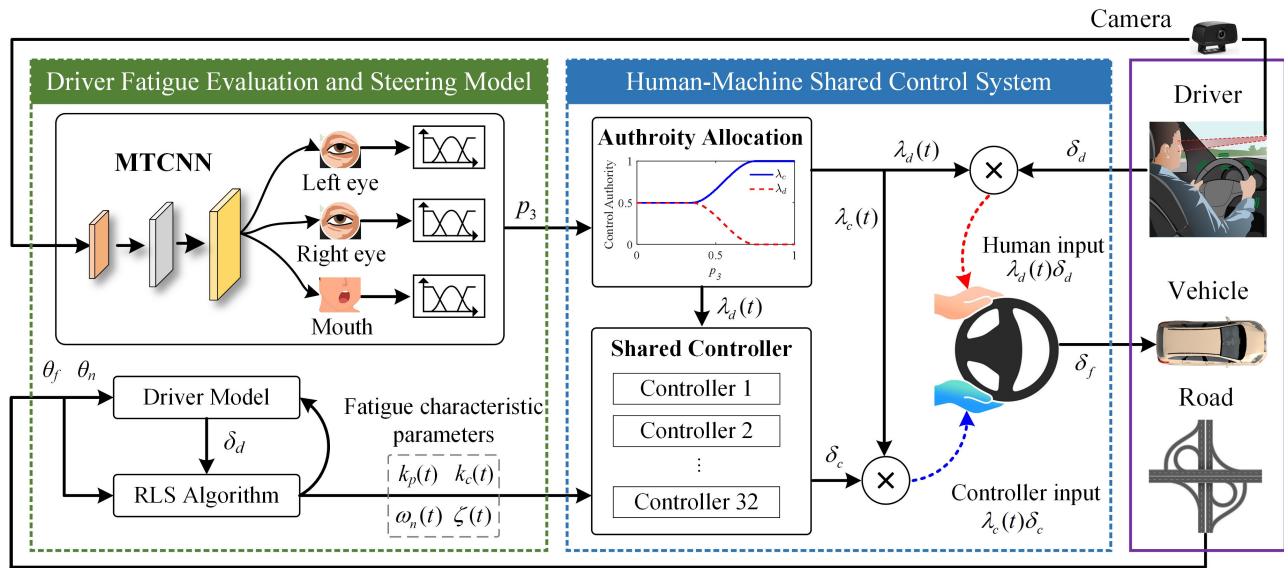


Fig. 8. Control framework of shared steering system.

to enhance the robustness of the shared control system. Meanwhile, the fuzzy rule method is used to adjust the control proportion of sub-controllers in real time to optimize the adaptability of the human-machine system. Ultimately, the steering angle δ_f applied to the front wheels of the vehicle is determined by the collaborative effort of the driver and the controller, as follows:

$$\delta_f = (\lambda_d(t)\delta_d + \lambda_c(t)\delta_c)r_g \quad (9)$$

In (9), δ_d signifies the steering wheel angle contributed by the driver through the steering column. Meanwhile, δ_c designates the steering angle provided by the controller. The authority levels of the driver and the controller to optimize their steering inputs are represented by $\lambda_d(t)$ and $\lambda_c(t)$. Additionally, r_g denotes the transmission ratio.

B. Fatigue-Based Authority Allocation Strategy

Given the dynamic interplay between the human and the machine, it becomes imperative to establish a judicious authority allocation strategy for co-driving vehicles, aimed at enhancing overall driving performance. Especially, the abnormal behavior caused by driver fatigue should be released by the authority allocation strategy. Therefore, a fatigue-based strategy is designed to allocate authority between the driver and controller through assessing the driver fatigue state in real time. When the driver is evaluated to be fatigued, the assistance controller will be allocated more authorities. As driver fatigue increases, a higher authority level is allocated to assistance controller [24]. When the driver's fatigue reaches the manually set threshold, the controller authority level will be set to 1. The driver's authority level will be limited to 0. On the contrary, when the driver is monitored to be awake, the driver's authority will be given the highest authority value. In this section, the strategy for allocating authority between the driver and controller is devised with three distinct modes, corresponding to situations of normal driving, medium fatigue, and severe

fatigue states, as follows:

$$\lambda_d(t) + \lambda_c(t) = 1 \quad (10-1)$$

$$\lambda_c(t) = \begin{cases} \lambda_d^{max} & 0 \leq p_3 \leq 0.35 \\ \varrho_0 + \varrho_1 p_3 + \varrho_2 p_3^2 + \varrho_3 p_3^3 & 0.35 < p_3 < 0.75 \\ 1 & 0.75 \leq p_3 \leq 1 \end{cases} \quad (10-2)$$

where λ_d and λ_c are applied directly to adjust steering inputs of the driver and controller. ϱ_i ($i = 0, 1, 2, 3$) denotes a constant that affects the shape of the curve λ_c . p_3 is the driver fatigue level obtained based on driver fatigue evaluation model. Note that the authority levels of the driver and the controller satisfy the following relationship of (10-1). The fatigue level range of $0 \leq p_3 \leq 0.35$ means the driver is in a normal state. In this paper, the normal driving state means that the driver has proficient driving skills and does not have symptoms such as fatigue. Therefore, the driver can be allocated a higher authority λ_d^{max} to satisfy his/her driving demands. λ_d^{max} is related to the road information. $0.35 < p_3 < 0.75$ indicates the driver is in a medium fatigue state. $0.75 \leq p_3 \leq 1$ represents the driver is in a severe fatigue state. It should be noted that the thresholds are obtained in Section II-B.

For drivers in the normal driving state and severe fatigue state, a fixed authority factor is adopted as the control authority allocation strategy. Under the normal driving state, the driver maintains his/her normal driving skills and the steering assistance system can release more control authority to him/her. On the other hand, when the driver is severely fatigued, the steering assistance system directly takes over the control authority. Drivers with a medium fatigue state are easily influenced by the external environment [28], [29], [43]. For instance, a driver may enter into a severe fatigue state due to a long-term driving task, or may return to a normal state due to psychological stress. Hence, to achieve a seamless transition of

authority, we employ a third-order polynomial curve method for crafting the authority allocation strategy in the case of medium fatigue. Additionally, as we contemplate the transitions between driver fatigue states, it becomes imperative to ensure the continuity and fluidity of the authority allocation strategy (10-2) across different states. Accordingly, boundary constraints are designed for the transition of different fatigue states, as follows:

$$\lambda_c(t)|_{p_3=0.35} = 0.5, \dot{\lambda}_c(t)|_{p_3=0.35} = 0 \quad (11-1)$$

$$\lambda_c(t)|_{p_3=0.75} = 1, \dot{\lambda}_c(t)|_{p_3=0.75} = 0 \quad (11-2)$$

The boundary constraints (11) are used to ensure that the control authority level is maintained and switched smoothly between different driving states. Therefore, ϱ_i ($i = 0, 1, 2, 3$) in (10-2) can be calculated by fitting optimization.

C. Shared Controller Design

We employ the widely recognized two-degree-of-freedom lateral dynamics vehicle model for the development of the steering controller, as described in [17].

$$\dot{v}_y = \frac{-2(C_f + C_r)}{mv_x} v_y + \frac{2(C_r l_r - C_f l_f) - mv_x^2}{mv_x} \gamma + \frac{2C_f}{m} \delta_f \quad (12-1)$$

$$\dot{\gamma} = \frac{2(C_r l_r - C_f l_f)}{M_z v_x} v_y + \frac{-2(C_f l_f^2 + C_r l_r^2)}{M_z v_x} \gamma + \frac{2C_f l_f}{M_z} \delta_f \quad (12-2)$$

In (12), v_y and γ denote the lateral velocity and yaw rate, respectively. δ_f is calculated by (9). The variables C_i ($i=f,r$) correspond to the cornering stiffness of the front and rear tires. Additionally, m and v_x signify the vehicle mass and vehicle speed, respectively. The parameters l_i ($i=f,r$) refer to the distances from the front and rear axles to the center of gravity. Moreover, M_z stands for the yaw moment of inertia. In the context of path tracking control, the lateral deviation model is obtained as follows, as detailed in [17].

$$\dot{y}_L = v_y + v_x \varphi_L + l_n \dot{\varphi}_L \quad (13-1)$$

$$\dot{\varphi}_L = \gamma - \rho_r v_x \quad (13-2)$$

where y_L stands for the lateral deviation at the driver's preview point, while φ_L denotes the heading deviation. The variable l_n represents the look-ahead distance. ρ_r denotes the road curvature of the reference path. In a co-driving vehicle system, the driver is always in the loop, which leads to the varying interaction behavior between human and machine in different fatigue states. To accurately understand the interaction behavior for the controller, a time-varying driver-vehicle interaction model for controller design is constructed by integrating equations (1), (2), (9), (12), and (13), as follows

$$\dot{\mathbf{x}} = \mathbf{A}(\boldsymbol{\rho})\mathbf{x} + \mathbf{B}_u(\boldsymbol{\rho})\mathbf{u} + \mathbf{B}_w(\boldsymbol{\rho})\mathbf{w} \quad (14)$$

where $\mathbf{x} = [v_y \ \gamma \ y_L \ \varphi_L \ \delta_d \ \dot{\delta}_d]^T$, $\mathbf{u} = \delta_c$, and $\mathbf{w} = \rho_r$. $\boldsymbol{\rho} = [\rho_1 \ \rho_2 \ \rho_3 \ \rho_4 \ \rho_5]^T$ of the model (14) includes the varying fatigue characteristic parameters and control authority level of a human driver. $\rho_1 = k_p(t)$, $\rho_2 = k_c(t)$, $\rho_3 = \zeta(t)$, $\rho_4 = w_n(t)$, $\rho_5 = \lambda_d(t)$. The fatigue characteristic parameters will be obtained in real-time by the RLS method. $\lambda_d(t)$ characterizes

the interaction behavior between the driver and controller in various fatigue states. This value is derived from the driver fatigue evaluation model. The matrices of the driver-vehicle interaction model (14) are given in Appendix B.

It becomes apparent that the time-varying model (14) relies significantly on the fatigue characteristics $\boldsymbol{\rho}$, potentially introducing system instability. From the perspective of engineering applications, due to the computational efficiency advantages of T-S fuzzy modeling for time-varying and nonlinear issues, it is employed to depict the time-varying attributes in (14), as demonstrated below.

$$\dot{\mathbf{x}} = \sum_{i=1}^{32} \eta_i (\mathbf{A}_i(\boldsymbol{\rho})\mathbf{x} + \mathbf{B}_{ui}(\boldsymbol{\rho})\mathbf{u} + \mathbf{B}_{wi}(\boldsymbol{\rho})\mathbf{w}) \quad (15-1)$$

$$\mathbf{z} = \sum_{i=1}^{32} \eta_i (\mathbf{C}_i(\boldsymbol{\rho})\mathbf{x} + \mathbf{D}_i(\boldsymbol{\rho})\mathbf{u} + \mathbf{E}_i(\boldsymbol{\rho})\mathbf{w}) \quad (15-2)$$

Here, \mathbf{z} represents the system's performance output. The variable η_i is introduced to capture the time-varying attributes of system (15), and it is determined by:

$$\eta_1 = \xi_{11}(\rho_1) * \xi_{12}(\rho_2) * \xi_{13}(\rho_3) * \xi_{14}(\rho_4) * \xi_{15}(\rho_5) \quad (16-1)$$

$$\eta_2 = \xi_{11}(\rho_1) * \xi_{12}(\rho_2) * \xi_{13}(\rho_3) * \xi_{14}(\rho_4) * \xi_{25}(\rho_5) \quad (16-2)$$

⋮

$$\eta_{32} = \xi_{21}(\rho_1) * \xi_{22}(\rho_2) * \xi_{23}(\rho_3) * \xi_{24}(\rho_4) * \xi_{25}(\rho_5) \quad (16-32)$$

where $\xi_{1i}(\rho_i)$ and $\xi_{2i}(\rho_i)$ are calculated by the following

$$\xi_{1i}(\rho_i) = \frac{\bar{\rho}_i - \rho_i}{\bar{\rho}_i - \underline{\rho}_i}, \xi_{2i}(\rho_i) = \frac{\rho_i - \underline{\rho}_i}{\bar{\rho}_i - \underline{\rho}_i} \quad (17)$$

$\bar{\rho}_i$ and $\underline{\rho}_i$ represent the upper and lower bounds of parameter ρ_i under different fatigue states, respectively. The boundaries of the fatigue characteristic parameters are shown in Table IV. Note that the lower and upper boundaries of the authority level $\lambda_d(t)$ are 0 and 1, respectively. $\mathbf{\Gamma}_i \in \{\mathbf{A}_i(\boldsymbol{\rho}), \mathbf{B}_{ui}(\boldsymbol{\rho}), \mathbf{B}_{wi}(\boldsymbol{\rho}), \mathbf{C}_i(\boldsymbol{\rho}), \mathbf{D}_i(\boldsymbol{\rho}), \mathbf{E}_i(\boldsymbol{\rho})\}$ represent system matrices of 32 parallel distributed subsystems. System matrices $\mathbf{\Gamma}_i$ can be obtained by replacing $\boldsymbol{\rho}$ with $\bar{\rho}_i$ and $\underline{\rho}_i$. Note that each parallel distributed subsystem is independent and linear time invariant.

To enhance driving comfort, tracking ability, and the cooperative performance of the shared steering controller, the performance output \mathbf{z} in equation (15) is formulated as $[a_y \ y_L \ \varphi_L \ \delta_d \ \dot{\delta}_d \ \lambda_d(t)\delta_d - \lambda_c(t)\delta_c]^T$. a_y is used to reflect the vehicle stability. y_L and φ_L are adopted to describe tracking performance. δ_d and $\dot{\delta}_d$ are introduced to guarantee a desired steering comfort [17]. $\lambda_d(t)\delta_d - \lambda_c(t)\delta_c$ is defined as the cooperative performance between the human driver and the steering controller [25]. Taking into account multiple objectives, including vehicle stability, path-tracking ability, steering comfort, and cooperative performance, and incorporating principles of H_∞ robust control theory, the performance objective function for the shared controller is established as follows, as indicated in [46].

$$J = \int_0^{+\infty} \mathbf{z}^T(t) \mathbf{Q} \mathbf{z}(t) dt \quad (18)$$

with $\mathbf{Q} = \text{diag}(q_1^s, q_2^s, q_3^s, q_4^s, q_5^s, q_6^s)$ and $s \in \{\text{ND}, \text{MF}, \text{SF}\}$. \mathbf{Q} represents the cost weighting matrix under different

fatigue levels. The optimization of the performance output z can take an alternative approach by fine-tuning the weighting coefficients q_i^s ($i=1, 2, \dots, 6$). The design form of the cost weighting matrix \mathbf{Q} in (18) is as follows.

- 1) q_1^s is used to adjust the vehicle stability performance in the controller design. In the practical application, q_1^s is set as three levels according to driver fatigue state. In the severely fatigued state, the vehicle stability is regarded as the most important factor in the controller design for the purpose of improving driving safety. Therefore, the weight coefficient of vehicle stability performance needs to satisfy the following relationship $q_1^{\text{SF}} > q_1^{\text{MF}} > q_1^{\text{ND}}$.
- 2) q_2^s and q_3^s are used to adjust the path-following performance in the controller design. Medium-fatigued drivers still are able to operate the vehicle. Vehicle stability is also not the most important indicator. In this case, the path-following ability is considered as the most important factor. Therefore, the weight coefficient of path-following performance needs to satisfy the following relationship $q_2^{\text{MF}} > q_2^{\text{SF}} > q_2^{\text{ND}}$ and $q_3^{\text{MF}} > q_3^{\text{SF}} > q_3^{\text{ND}}$.
- 3) q_4^s and q_5^s are used to adjust the steering comfort performance. The low driving workload is the basic requirement for drivers in the normal state. To this end, the weight coefficient of steering comfort performance is designed to satisfy the following relationship $q_4^{\text{ND}} > q_4^{\text{MF}} > q_4^{\text{SF}}$ and $q_5^{\text{ND}} > q_5^{\text{MF}} > q_5^{\text{SF}}$.
- 4) q_6^s aims to optimize the steering cooperative performance to reduce human-machine conflicts. The weight coefficient of steering cooperative performance is designed to satisfy the following relationship $q_6^{\text{ND}} > q_6^{\text{MF}} > q_6^{\text{SF}}$, since the normal driver is expected to be able to operate the vehicle in a cooperative manner with the steering assistance system.

The steering compensation u of the fuzzy system (15) based on state-feedback control method can be calculated by

$$u = \sum_{i=1}^{32} \eta_i \mathbf{K}_i x \quad (19)$$

Here, \mathbf{K}_i represents the control gain for each parallel distributed subsystem. To solve the robust optimal control problem (ROCP) of the T-S fuzzy system, z should meet the condition $\|z\|_2 < \hbar \|w\|_2$. \hbar is a positive value for mitigating disturbances w . ROCP can be realized based on the following theorem.

Theorem 1: The T-S fuzzy driver-vehicle interaction system described by (15) possesses a state-feedback H_∞ controller if and only if there exist symmetric positive definite matrices $\mathbf{\Xi}$ and \mathfrak{R}_i ($i = 1, 2, \dots, 32$) that ensure the satisfaction of the following linear matrix inequalities (LMIs):

$$\begin{bmatrix} \mathbf{\Pi}(A_i(\rho)\mathbf{\Xi} + B_{ui}(\rho)\mathfrak{R}_i + \epsilon\mathbf{\Xi})B_{wi}(\rho)\tilde{\Psi}_i \\ \star & -\hbar\mathbf{I} & \mathbf{W}_i \\ \star & \star & -\mathbf{I} \end{bmatrix} < 0 \quad (20)$$

where $\mathbf{\Pi}(X) = X + X^T$, $\tilde{\Psi}_i = [\mathbf{\Xi}^T C_i^T(\rho) + \mathfrak{R}_i^T D_i^T(\rho)](\mathbf{Q})^{\frac{1}{2}}$ and $\mathbf{W}_i = E_i^T(\rho)(\mathbf{Q})^{\frac{1}{2}}$. \star denotes the matrices that can be deduced by symmetry. **Proof:** The proof is given in Appendix C.

Then, the state-feedback control gain \mathbf{K}_i in each parallel distributed subsystem (15) and (19) is calculated as

$$\mathbf{K}_i = \mathfrak{R}_i \mathbf{\Xi}^{-1} \quad (21)$$

Ensuring the compliance with the output and control input restrictions in the driver-vehicle interaction system (15) presents an invariant set challenge, as discussed in [46]. To address this issue, the robust set-invariance property is introduced, denoted as **Theorem 2** and **3**. In the pursuit of enhancing system safety in real-world applications, the controller design takes into account the output constraints of the driver-vehicle interaction system, conforming to the following limits.

$$-v_{y\max} \leq v_y \leq v_{y\max} \quad (22-1)$$

$$-\gamma_{\max} \leq \gamma \leq \gamma_{\max} \quad (22-2)$$

$$-y_{L\max} \leq y_L \leq y_{L\max} \quad (22-3)$$

$$-\varphi_{L\max} \leq \varphi_L \leq \varphi_{L\max} \quad (22-4)$$

Theorem 2: Under the assumption that the initial condition $x(0)$ is known, the constraints $\|x_i\| \leq \varepsilon_i$ are always guaranteed when the following LMIs hold [46].

$$\begin{bmatrix} 1 & x^T(0) \\ x(0) & \mathbf{\Xi} \end{bmatrix} \geq 0 \quad (23-1)$$

$$\begin{bmatrix} \mathbf{\Xi} & \mathbf{\Xi} d_i^T \\ d_i \mathbf{\Xi} & \varepsilon_i^2 \mathbf{I} \end{bmatrix} \geq 0 \quad (23-2)$$

Here, $\mathbf{\varepsilon} = [v_{y\max}, \gamma_{\max}, y_{L\max}, \varphi_{L\max}]$. d_i is the unit vector, adhering to the condition $x_i = d_i x$. Furthermore, the controller design must take into account the steering constraint, ensuring that the compensation u falls within the following limits:

$$-u_{\max} \leq u \leq u_{\max} \quad (24)$$

Theorem 3: Assuming that the initial condition $x(0)$ is known, it is assured that the constraint $\|u\|_2 \leq u_{\max}$ is always met provided the LMIs are satisfied, as discussed in [46].

$$\begin{bmatrix} \mathbf{\Xi} & \mathfrak{R}_i^T \\ \mathfrak{R}_i & u_{\max}^2 \mathbf{I} \end{bmatrix} \geq 0 \quad (25)$$

Remark 1: Given a parameter ϵ , the steering compensation (19) achieves asymptotic stability concerning (15) through the minimization of the objective performance function (18), under the condition that there exists a positive definite matrix $\mathbf{\Xi}$, \mathbf{K}_i ($i=1, 2, \dots, 32$), and a positive scalar \hbar . This condition is met when addressing the sub-optimization control problem as follows:

$$\begin{aligned} & \text{Min } \hbar \\ & \text{s.t. (20), (23) and (25)} \end{aligned} \quad (26)$$

IV. DRIVER-IN-THE-LOOP TEST

A. Experimental Setup

A driving simulator platform is built to verify the performance of the controller, as shown in Fig. 9. The driving simulator platform primarily encompasses components such as the road environment, driver fatigue evaluation system, real-time controller, and vehicle dynamics model. A virtual

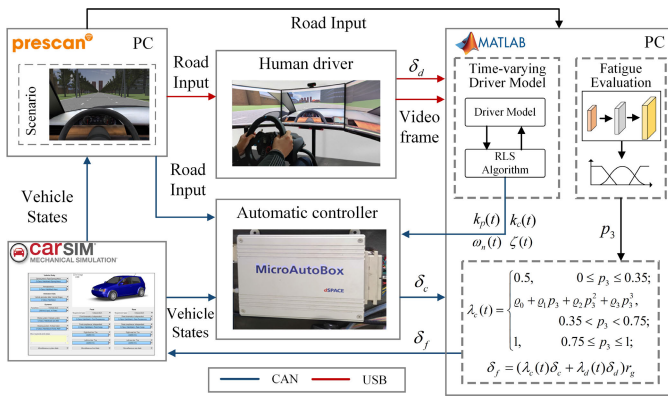


Fig. 9. Driving simulator test platform.

TABLE V
VEHICLE DYNAMICS PARAMETERS

Parameter	Definition	Value
m	Mass	1705 kg
M_z	Yaw moment of inertia	3048 kg · m ²
l_f	Front wheelbase	1.035 m
l_r	Rear wheelbase	1.665 m
C_f	Front tire cornering stiffness	103130 N/rad
C_r	Rear tire cornering stiffness	73854 N/rad

driving environment is established through the utilization of PreScan software integrated into the PC. A low-cost Logitech C270 RGB camera is adapted to capture volunteers' face images. The algorithm of the driver fatigue evaluation system is programmed in Python with TensorFlow 2.0 package and runs on an Intel i5-7300HQ 2.5GHz CPU. The facial images are transmitted to the PC through the USB protocol. In addition, time-varying driver fatigue characteristics and authority levels are identified through Matlab in PC, respectively. Then, the fatigue characteristic parameters and vehicle states are conveyed to the real-time dSPACE controller through the CAN bus. The fuzzy shared control algorithm, as elaborated in Section IV, is executed on the real-time dSPACE platform to facilitate rapid function prototyping. The steering inputs from both entities are combined linearly, taking into account human-machine authority levels. The outcome of the human-machine control is implemented in the high-fidelity Carsim vehicle dynamics model. In this experimental validation, the vehicle parameters are detailed in Table V.

In this experiment, Applus IDIADA serves as the testing scenario, as illustrated in Fig. 10. For the large-curvature road, the driver's workload is directly reflected by steering behavior. In the experimental scenario of this paper, the range of the steering wheel angle is between 150° and 200°, when the driver is passing through continuous curves without assistance. If the steering wheel angle is completely imposed by the driver, the vehicle will have a greater risk of deviation or even instability in a scenario where the average vehicle speed is 20 m/s and the turning radius is between 50 and 100 m. In addition, from the perspective of driver workload, the driver's steering angle is expected to be less than 90° under the large curvature scenario. Thus, during the normal driving state,

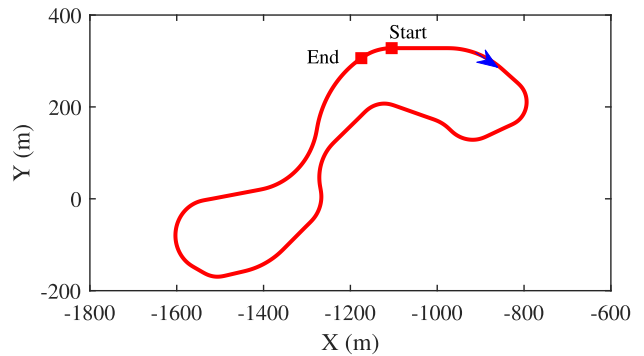


Fig. 10. The test scenario.

the driver's authority level λ_d^{max} is set to 0.5, which can satisfy our requirements of human-machine shared vehicles. To point out the performance of the proposed shared control method, we engage fifteen drivers with varying levels of fatigue in the experiment. The specific testing requirements for the drivers are outlined in Section II-C.

B. Experimental Validation

To assess shared control performance, four evaluation indices are given to analyze the human-machine conflict level as J_1 , driving comfort as J_2 , vehicle stability as J_3 , and path-tracking performance as J_4 [5], [17], [21].

$$J_1 = \frac{T_C}{T_S}, \quad T_C = \{t \in [0, T_S] : \tilde{\delta}_d \cdot \tilde{\delta}_c < 0\} \quad (27-1)$$

$$J_2 = \frac{\int_{T_S} \tilde{\delta}_{total}^2(t) + \dot{\tilde{\delta}}_{total}^2(t) dt}{T_S} \quad (27-2)$$

$$J_3 = \frac{\int_{T_S} a_y^2(t) dt}{T_S} \quad (27-3)$$

$$J_4 = \frac{\int_{T_S} e_y^2(t) dt}{T_S} \quad (27-4)$$

In (27), T_S represents the test duration, while T_C denotes the duration of the conflict behavior between the controller and the driver. The effective steering wheel angles of the driver and controller, denoted as $\tilde{\delta}_d$ and $\tilde{\delta}_c$, are calculated as $\tilde{\delta}_d = \lambda_d(t)\delta_d$ and $\tilde{\delta}_c = \lambda_c(t)\delta_c$. The combined effective steering angle, $\tilde{\delta}_{total}$, is the result of superimposing the steering angles of both the human and the controller. Additionally, e_y represents the lateral deviation of the vehicle from the desired trajectory, which can be computed using (13), given that l_n is set to 0.

A larger value of J_1 implies a higher level of conflict between the two participants, which will reduce the quality of human-machine interaction. J_2 encompasses the driver's physical workload and psychological stress. A lower value of J_2 suggests that the driver experiences reduced workload and psychological strain while conducting driving tasks. Smaller values for both J_3 and J_4 indicate improved vehicle stability and path-following performance.

For convenience, the proposed shared controller is denoted as DRSSC. The benchmark controller without considering time-varying driver fatigue characteristics is denoted as SSC,

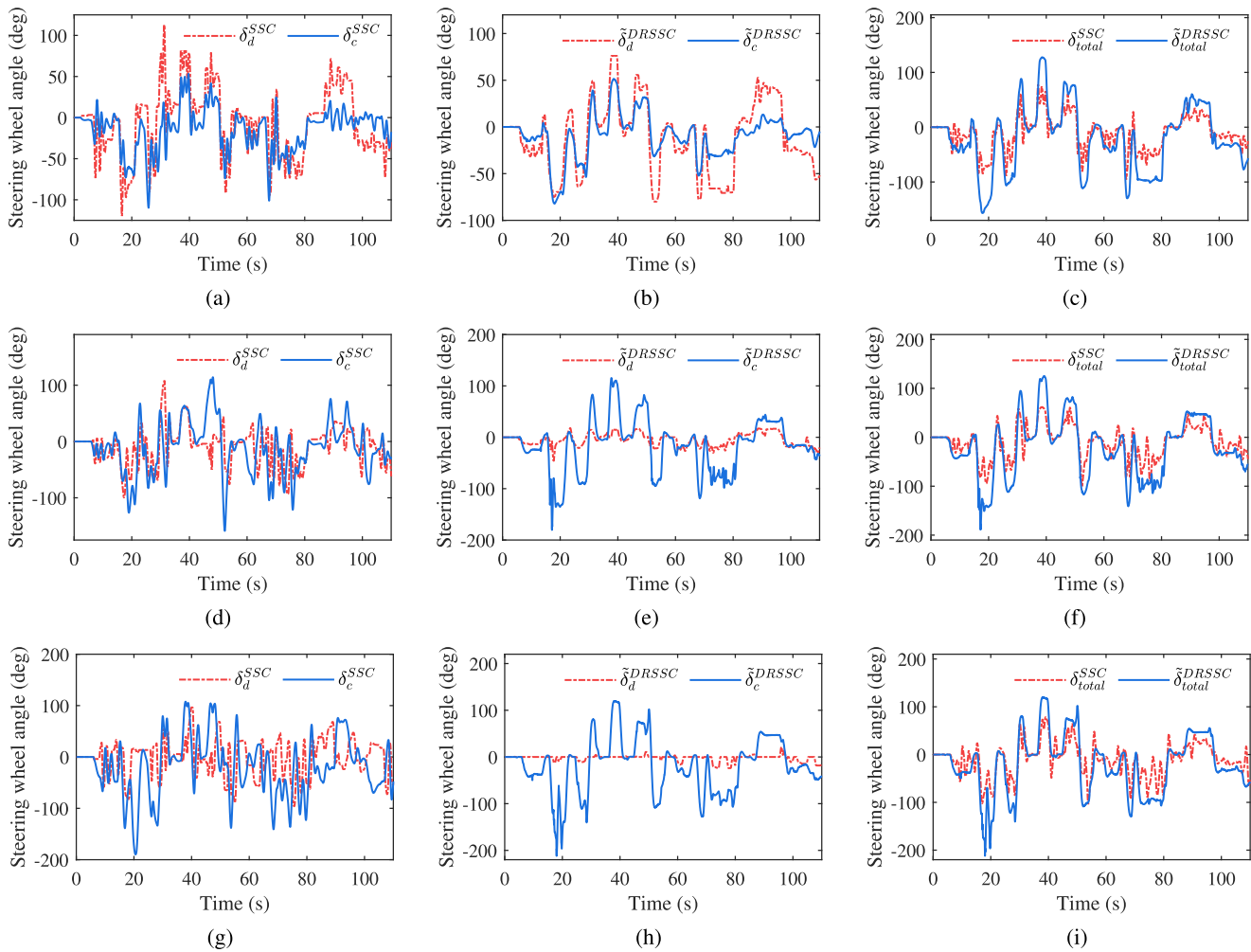


Fig. 11. The human-machine steering response under different fatigue levels: (a)-(c) State A; (d)-(f) State B; (g)-(i) State C. δ_d^{SSC} and δ_c^{SSC} represent the effective steering angles of the human and the machine with the assistance of SSC, respectively. $\tilde{\delta}_d^{DRSSC}$ and $\tilde{\delta}_c^{DRSSC}$ indicate the effective steering angles of the human and the machine with the assistance of DRSSC, respectively. δ_{total}^{SSC} is the superposition of steering angles of the human and the machine with the assistance of SSC. $\tilde{\delta}_{total}^{DRSSC}$ is the effective superposition of steering angles of the human and the machine with the assistance of DRSSC, respectively.

which is based on the robust state-feedback method. In addition, $\lambda_c(t)$ and $\lambda_d(t)$ in SSC are set as 0.5 and 0.5, respectively. However, the authority levels of DRSSC can be adjusted according to driver fatigue states. The quantitative performance indices of both controllers are shown in Table VI. It should be noted that the quantitative performance indices are average results of fifteen drivers. In order to intuitively show the control performance, the testing results of both controllers under three different fatigue states are compared in terms of the human-machine interaction and vehicle performance, as shown in Figs. 11 and 12.

As the driver fatigue level increases, the driver's ability to control the vehicle decreases, mainly in the form of constantly adjusting the steering wheel. With the assistance of SSC that does not consider time-varying driver fatigue characteristics, the controller will have obvious jittery as shown in Fig. 11 (a), (d), and (g), which severely reduces the quality of human-machine interaction and driving comfort.

On the contrary, considering the time-varying driving fatigue state, the DRSSC proposed in this paper can give an effective control authority allocation strategy to suppress the misoperation behavior caused by a fatigued driver, as shown in

TABLE VI
RESULTS OF THE PERFORMANCE INDICES

State Type	Control Type	J_1	J_2	J_3	J_4
State A	DRSSC	0.23	61.5	213.4	5.1
	SSC	0.27	64.8	232.8	5.7
Performance Improvement Rate (%)		15%	5%	8%	11%
State B	DRSSC	0.24	66.2	223.1	11.2
	SSC	0.30	79.2	250.5	37.5
Performance Improvement Rate (%)		20%	16%	11%	70%
State C	DRSSC	0.23	68.2	221.3	2.8
	SSC	0.40	89.5	263.7	48.5
Performance Improvement Rate (%)		43%	21%	16%	94%

Fig. 12 (c), (f) and (i). The human-machine authority calculated based on the DFEM weakens the steering input of the fatigued driver, as shown in Fig. 11 (b), (e), and (h). Therefore, the steering compensation of DRSSC is smoother than that of SSC. When the driver shows severe fatigue states such as frequent blinking and yawning, the DFEM determines that the driver is no longer competent for the driving task. Therefore, the driver's control authority is given as 0 and the controller's authority is given as 1. It can also be seen from Fig. 11 (h)

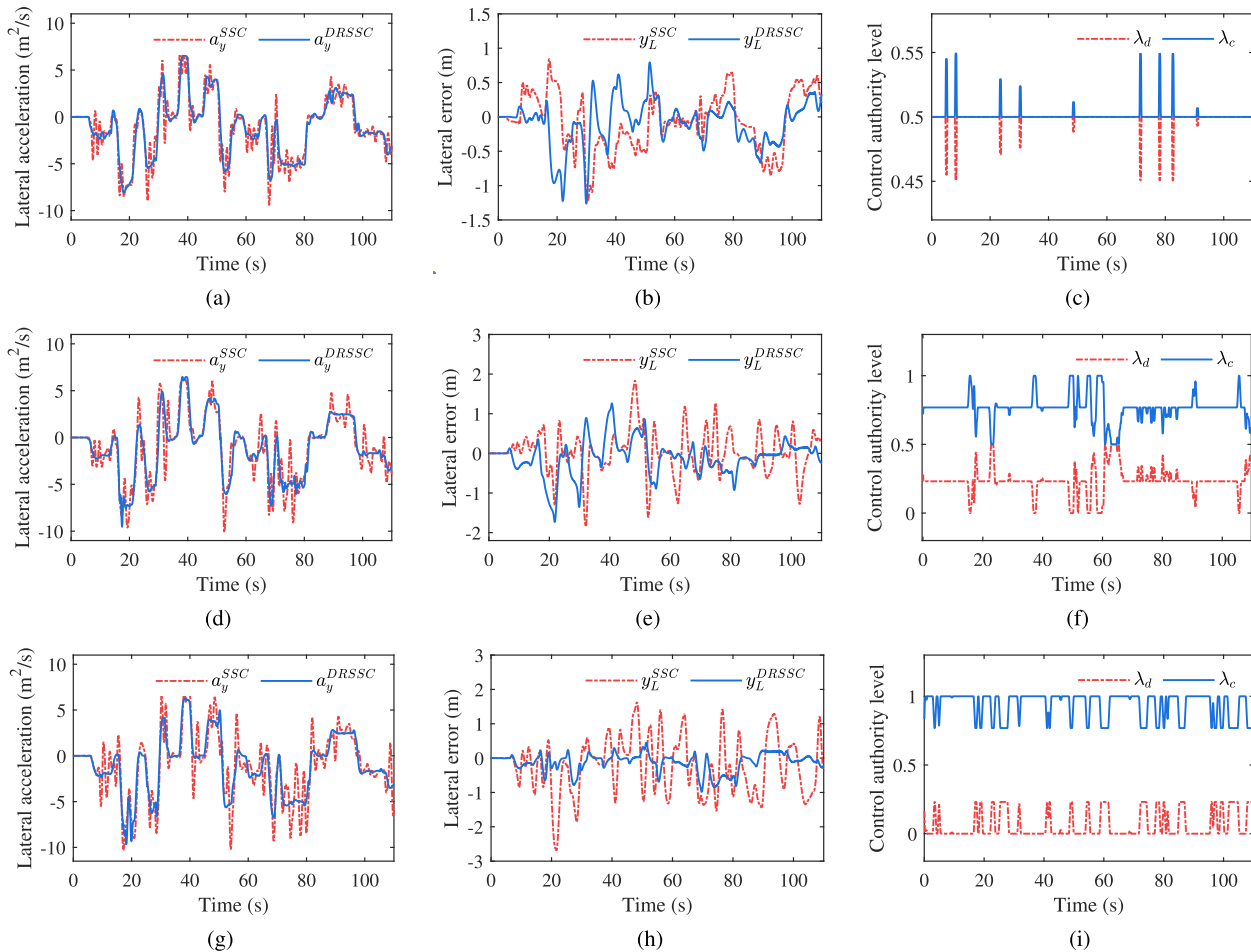


Fig. 12. Lateral acceleration, lateral deviation and control authority with different controllers: (a)-(c) State A; (d)-(f) State B; (g)-(i) State C. a_y^{SSC} and y_L^{SSC} represent the lateral acceleration and the lateral deviation with the assistance of SSC, respectively. a_y^{DRSSC} and y_L^{DRSSC} mean the lateral acceleration and the lateral deviation with the assistance of DRSSC, respectively. λ_d and λ_c represent the allocated authorities of the human and the machine, respectively.

that the driver's effective steering wheel angle is almost 0° and there is no longer a valid input to the vehicle steering system. Fig. 11 (c), (f), and (i) demonstrate that the effective human-machine steering wheel angle with the assistance of DRSSC is smoother than that of SSC controller, which means that the driving comfort is improved.

According to the performance index J_2 in Table VI, driving comfort under three different fatigue levels is improved by more than 5% with the assistance of DRSSC. In particular, the jitter frequency and jitter amplitude of the human-machine total steering input are significantly reduced under severely fatigued driving. The proposed control strategy enhances driving comfort by 21% when compared to the robust state feedback control strategy that does not account for fatigue characteristics. In addition, from the performance index J_1 of Table VI, it can be found that the human-machine conflict level is reduced by more than 15%, which improves the quality of human-machine interaction. In particular, the human-machine conflict level is reduced by more than 43% by the proposed controller under the severe driver fatigue state.

The results of lateral acceleration a_y are shown in Fig. 12 (a), (d), and (g). It can be found that the value of a_y under State B and C is larger than that of State A, which means that the driver's fatigued steering behavior deteriorates

the vehicle stability. Especially, with the assistance of SSC, the value of a_y under State B and C has been more than $10 \text{ m}^2/\text{s}^2$. In addition, the driver in a severe fatigue state has frequent jitter when steering the vehicle, which causes a large value of lateral acceleration. In contrast, the DRSSC proposed in this paper attenuates the effect of fatigue driving behavior and maintains the vehicle stability. It is obvious that the lateral acceleration of the vehicle is significantly smaller and smoother with the assistance of DRSSC. According to the performance index J_3 in Table VI, the vehicle stability under severe fatigue level is improved by 16% with the assistance of DRSSC.

As can be seen in Fig. 12 (b), when the driver in State A is tracking the desired path with the assistance of both controllers, the vehicle's maximum lateral deviations are about 1.2 m, and the overall lateral deviation is at about 0.5 m. In normal driving mode, the ratio of human-machine control authority under both control methods is close to 1:1. Therefore, the difference between the two controllers in path tracking performance is not significant. As shown in Table VI, the path-tracking performance indices of the two controllers are 5.1 and 5.7, respectively.

From Fig. 12 (e) and (h), it can be found that for the driver in the States B and C with higher fatigue levels, the SSC control

strategy cannot effectively reduce the lateral deviation of the vehicle, in which the maximum lateral deviation has exceeded 2 m. The controller proposed in this paper can dynamically coordinate the control authority between the human and the machine. The controller's authority is strengthened during fatigue driving, thereby enhancing the vehicle's ability to track its path. According to the performance index J_4 presented in Table VI, the path-tracking performance significantly improves by over 70% with the assistance of DRSSC under higher levels of driver fatigue. In summary, the experiments demonstrate that the designed human-machine shared control approach can yield superior driving performance across drivers experiencing varying degrees of fatigue.

V. CONCLUSION

In this paper, we propose a fatigue-based human-machine shared control framework to tackle the challenge of suboptimal driving performance under varying levels of driver fatigue. To achieve this, we first build a time-varying driver steering model, which effectively captures driver behavior. And the driver fatigue evaluation system is established by extracting the facial features to determine the fatigue level. Furthermore, the driver characteristic parameters are analyzed under different fatigue states. Then, the allocation of human-machine control authority is determined based on the evaluation of driver fatigue states to mitigate any abnormal driver behavior. Following this, the robust shared control approach is employed for counteracting external disturbances. Finally, a set of quantified performance indices for the shared controller is devised to assess performance via a driver-in-the-loop simulator. The outcomes demonstrate a substantial enhancement in driving performance across various fatigue levels thanks to the proposed strategy.

In future endeavors, considering that the driving fatigue state will affect the driver's attention on the road, the driver distraction characteristics should be also analyzed. Additionally, the human-machine shared control framework outlined in this paper will be subjected to real-world validation within actual vehicle setups.

APPENDIX A PARAMETERS OF STANDARD LEAST SQUARES REGRESSION MODEL

The parameters of the standard least squares regression model (3) is given as follows:

$$\begin{cases} b_1 = a_1/a_2, & b_2 = a_0/a_2, \\ b_3 = k_p(t)/a_2, & b_4 = k_c(t)/a_2. \end{cases} \quad (\text{A-1})$$

$$\begin{cases} a_0 = \frac{4}{\Delta t^2} - \frac{4}{\Delta t} \zeta(t)w_n(t) + w_n^2(t), \\ a_1 = -\frac{8}{\Delta t^2} + 2w_n^2(t), \\ a_2 = \frac{4}{\Delta t^2} + \frac{4}{\Delta t} \zeta(t)w_n(t) + w_n^2(t). \end{cases} \quad (\text{A-2})$$

$$\begin{cases} u_f = \theta_{f,k} + 2\theta_{f,k-1} + \theta_{f,k-2}, \\ u_n = \theta_{n,k} + 2\theta_{n,k-1} + \theta_{n,k-2}. \end{cases} \quad (\text{A-3})$$

where Δt is sampling time.

APPENDIX B MATRICES OF DRIVER-VEHICLE INTERACTION MODEL

The coefficient matrices in the model (14) can be obtained as

$$\mathbf{A}(\rho) = \begin{bmatrix} a_{11} & a_{12} & 0 & 0 & \lambda_d(t)b_{u1} & 0 \\ a_{21} & a_{22} & 0 & 0 & \lambda_d(t)b_{u2} & 0 \\ 1 & l_n & 0 & v_x & 0 & 0 \\ 0 & 1 & 0 & 0 & 0 & 0 \\ 0 & 0 & 0 & 0 & 1 & 0 \\ 0 & 0 & a_{63} & a_{64} & a_{65} & a_{66} \end{bmatrix} \quad (\text{B-1})$$

$$\mathbf{B}_u(\rho) = [\lambda_c(t)b_{u1} \ \lambda_c(t)b_{u2} \ 0 \ 0 \ 0 \ 0]^T \quad (\text{B-2})$$

$$\mathbf{B}_w(\rho) = [0 \ 0 \ -v_x l_n \ -v_x \ 0 \ r_g k_p(t) l_{far}]^T \quad (\text{B-3})$$

where

$$\begin{cases} a_{11} = \frac{-2(C_f + C_r)}{mv_x}, \\ a_{12} = \frac{2(C_r l_r - C_f l_f) - mv_x^2}{2(C_r l_r - C_f l_f)}, \\ a_{21} = \frac{2(C_r l_r - C_f l_f)}{M_z v_x}, \\ a_{22} = \frac{-2(C_f l_f^2 + C_r l_r^2)}{M_z v_x}, \\ a_{63} = -\frac{r_g k_c(t)}{l_n}, \quad a_{64} = -r_g k_c(t), \\ a_{65} = -w_n^2(t), \quad a_{66} = -2\zeta(t)w_n(t), \\ b_{u1} = \frac{2C_f}{m}, \quad b_{u2} = \frac{2C_f l_f}{M_z}. \end{cases} \quad (\text{B-4})$$

APPENDIX C THE PROOF OF THEOREM 1

To demonstrate the quadratic stability of the closed-loop system (15), a Lyapunov function is introduced as follows:

$$\ell(\mathbf{x}) = \mathbf{x}^T \mathbf{\Lambda} \mathbf{x} \quad (\text{C-1})$$

where $\mathbf{\Lambda}$ is a positive definite matrix. System stability must be guaranteed by the Lyapunov function (C-1), which should fulfill the following inequality:

$$\dot{\ell}(\mathbf{x}) + \mathbf{z}^T \mathbf{Q} \mathbf{z} < \hbar w^T w - 2\epsilon \ell(\mathbf{x}) \quad (\text{C-2})$$

Taking ϵ as a positive scalar into account, by integrating both sides of (C-2), we can derive the inequality:

$$\int_0^{+\infty} \mathbf{z}^T(t) \mathbf{Q} \mathbf{z}(t) dt < \ell(0) - \ell(\infty) + \hbar \int_0^{+\infty} w^T(t) w(t) dt \quad (\text{C-3})$$

Subsequently, we can determine the upper limit of the objective performance function (18) as follows:

$$J < \ell(0) + \hbar W_{max} \quad (\text{C-4})$$

In (C-4), the positive scalar W_{max} represents the maximum value of the external disturbance w^2 . Given $\ell(0)$ and W_{max} , the minimization of the scalar \hbar allows us to minimize J . By substituting equations (15) and (19) into (C-2), we can

rewrite the matrix inequality as follows:

$$\begin{aligned} \Omega &= \dot{\mathbf{x}}^T \Lambda \mathbf{x} + \mathbf{x}^T \Lambda \dot{\mathbf{x}} + \mathbf{z}^T \mathbf{Q} \mathbf{z} - \dot{h} w^T w + 2\epsilon \ell(\mathbf{x}) \\ &= \sum_{i=1}^{i=32} \eta_i (\mathbf{U}(Y^T \Lambda \mathbf{x} + \epsilon \mathbf{x}^T \Lambda \mathbf{x}) + \mathbf{z}^T \mathbf{Q} \mathbf{z}) - \dot{h} w^T w < 0 \end{aligned} \quad (\text{C-5})$$

where $Y=[A_i(\rho)+B_{ui}(\rho)K_i]x+B_{wi}(\rho)w$. The matrix inequality (C-5) can be derived as

$$\Omega = \sum_{i=1}^{i=32} \eta_i \begin{bmatrix} \mathbf{x} \\ \mathbf{w} \end{bmatrix}^T \Theta_i \begin{bmatrix} \mathbf{x} \\ \mathbf{w} \end{bmatrix} < 0 \quad (\text{C-6})$$

Inequality (C-6) can be satisfied if the following inequality holds

$$\Theta_i = \begin{bmatrix} \$ & \Lambda B_{wi}(\rho) \\ \star & -\dot{h} I \end{bmatrix} + G_i^T G_i < 0 \quad (\text{C-7})$$

where $\$ = \mathbf{U}(\Lambda A_i(\rho) + \Lambda B_{ui}(\rho)K_i + \epsilon \Lambda)$ and $G_i = (\mathbf{Q})^{\frac{1}{2}} [C_i(\rho) + D_i(\rho)K_i \ E_i(\rho)]$. Referring to Schur complement lemma [46], the matrix inequality (C-7) can be converted as

$$\begin{bmatrix} \$ & \Lambda B_{wi}(\rho) & \Psi_i \\ \star & -\dot{h} I & W_i \\ \star & \star & -I \end{bmatrix} < 0 \quad (\text{C-8})$$

where $\Psi_i = [C_i^T(\rho) + K_i^T D_i^T(\rho)](\mathbf{Q})^{\frac{1}{2}}$. Note that (C-8) consists of nonlinear matrix inequalities. To handle this, we'll use a substitution method to transform (C-8) into LMIs. We define $\Xi = \Lambda^{-1}$ to linearize (C-8). To further linearize it, a new variable is introduced as follows:

$$\mathfrak{R}_i = K_i \Xi \quad (\text{C-9})$$

By left-multiplying with $\text{diag}(\Xi, I, I)$ and right-multiplying with $\text{diag}(\Xi^{-1}, I, I)$, we can derive the LMIs (20). This confirms the validity of *Theorem 1* and concludes the proof.

REFERENCES

- [1] D. Chu, H. Li, C. Zhao, and T. Zhou, "Trajectory tracking of autonomous vehicle based on model predictive control with PID feedback," *IEEE Trans. Intell. Transp. Syst.*, vol. 24, no. 2, pp. 2239–2250, Feb. 2023.
- [2] C. Huang, C. Lv, P. Hang, Z. Hu, and Y. Xing, "Human-machine adaptive shared control for safe driving under automation degradation," *IEEE Intell. Transp. Syst. Mag.*, vol. 14, no. 2, pp. 53–66, Mar. 2022.
- [3] H. Deng, Y. Zhao, S. Feng, Q. Wang, and F. Lin, "Shared control for intelligent vehicle based on handling inverse dynamics and driving intention," *IEEE Trans. Veh. Technol.*, vol. 71, no. 3, pp. 2706–2720, Mar. 2022.
- [4] H. E. B. Russell, L. K. Harbott, I. Nisky, S. Pan, A. M. Okamura, and J. C. Gerdes, "Motor learning affects car-to-driver handover in automated vehicles," *Sci. Robot.*, vol. 1, no. 1, Dec. 2016, Art. no. eaah5682.
- [5] A. Benloucif, A.-T. Nguyen, C. Sentouh, and J.-C. Popieul, "Cooperative trajectory planning for haptic shared control between driver and automation in highway driving," *IEEE Trans. Ind. Electron.*, vol. 66, no. 12, pp. 9846–9857, Dec. 2019.
- [6] W. Wang et al., "Decision-making in driver-automation shared control: A review and perspectives," *IEEE/CAA J. Autom. Sinica*, vol. 7, no. 5, pp. 1289–1307, Sep. 2020.
- [7] J. Xie, X. Xu, F. Wang, Z. Liu, and L. Chen, "Coordination control strategy for human-machine cooperative steering of intelligent vehicles: A reinforcement learning approach," *IEEE Trans. Intell. Transp. Syst.*, vol. 23, no. 11, pp. 21163–21177, Nov. 2022.
- [8] J. Liang et al., "A distributed integrated control architecture of AFS and DYC based on MAS for distributed drive electric vehicles," *IEEE Trans. Veh. Technol.*, vol. 70, no. 6, pp. 5565–5577, Jun. 2021.
- [9] N. Ahmadian, A. Khosravi, and P. Sarhadi, "Driver assistant yaw stability control via integration of AFS and DYC," *Vehicle Syst. Dyn.*, vol. 60, no. 5, pp. 1742–1762, Jan. 2021.
- [10] Z. Ercan, A. Carvalho, M. Gokasan, and F. Borrelli, "Modeling, identification, and predictive control of a driver steering assistance system," *IEEE Trans. Hum.-Mach. Syst.*, vol. 47, no. 5, pp. 700–710, Oct. 2017.
- [11] Z. Ercan, A. Carvalho, H. E. Tseng, M. Gokasan, and F. Borrelli, "A predictive control framework for torque-based steering assistance to improve safety in highway driving," *Vehicle Syst. Dyn.*, vol. 56, no. 5, pp. 810–831, Jun. 2017.
- [12] Y. Chen, C. Stout, A. Joshi, M. L. Kuang, and J. Wang, "Driver-assistance lateral motion control for in-wheel-motor-driven electric ground vehicles subject to small torque variation," *IEEE Trans. Veh. Technol.*, vol. 67, no. 8, pp. 6838–6850, Aug. 2018.
- [13] Z. Li, H. Chen, H. Liu, P. Wang, and X. Gong, "Integrated longitudinal and lateral vehicle stability control for extreme conditions with safety dynamic requirements analysis," *IEEE Trans. Intell. Transp. Syst.*, vol. 23, no. 10, pp. 19285–19298, Oct. 2022.
- [14] Y. Yan, J. Wang, K. Zhang, Y. Liu, Y. Liu, and G. Yin, "Driver's individual risk perception-based trajectory planning: A human-like method," *IEEE Trans. Intell. Transp. Syst.*, vol. 23, no. 11, pp. 20413–20428, Nov. 2022.
- [15] X. Tang, B. Huang, T. Liu, and X. Lin, "Highway decision-making and motion planning for autonomous driving via soft actor-critic," *IEEE Trans. Veh. Technol.*, vol. 71, no. 5, pp. 4706–4717, May 2022.
- [16] Y. Jiang, W. Deng, J. Wu, S. Zhang, and H. Jiang, "Adaptive steering feedback torque design and control for driver-vehicle system considering driver handling properties," *IEEE Trans. Veh. Technol.*, vol. 68, no. 6, pp. 5391–5406, Jun. 2019.
- [17] J. Wang, Z. Fang, M. Dai, G. Yin, J. Xia, and P. Li, "Robust steering assistance control for tracking large-curvature path considering uncertainties of driver's steering behavior," *Proc. Inst. Mech. Eng., D, J. Automobile Eng.*, vol. 235, no. 7, pp. 2013–2028, Jun. 2021.
- [18] S. Kolekar, J. de Winter, and D. Abbink, "Human-like driving behaviour emerges from a risk-based driver model," *Nature Commun.*, vol. 11, no. 1, pp. 1–13, Sep. 2020.
- [19] R. Li, Y. Li, S. E. Li, C. Zhang, E. Burdet, and B. Cheng, "Indirect shared control for cooperative driving between driver and automation in steer-by-wire vehicles," *IEEE Trans. Intell. Transp. Syst.*, vol. 22, no. 12, pp. 7826–7836, Dec. 2021.
- [20] R. Li, S. Li, H. Gao, K. Li, B. Cheng, and D. Li, "Effects of human adaptation and trust on shared control for driver-automation cooperative driving," SAE Int., Warrendale, PA, USA, Tech. Rep. 2017-01-1987, Sep. 2017. [Online]. Available: <https://doi.org/10.4271/2017-01-1987>.
- [21] M. Li et al., "A two-layer potential-field-driven model predictive shared control towards driver-automation cooperation," *IEEE Trans. Intell. Transp. Syst.*, vol. 23, no. 5, pp. 4415–4431, May 2022.
- [22] Z. Shi, H. Chen, T. Qu, and S. Yu, "Human-machine cooperative steering control considering mitigating human-machine conflict based on driver trust," *IEEE Trans. Hum.-Mach. Syst.*, vol. 52, no. 5, pp. 1036–1048, Oct. 2022.
- [23] M. Marcano, S. Díaz, J. Pérez, and E. Irigoyen, "A review of shared control for automated vehicles: Theory and applications," *IEEE Trans. Hum.-Mach. Syst.*, vol. 50, no. 6, pp. 475–491, Dec. 2020.
- [24] S. Zhou, Z. Ju, Y. Liu, H. Zhang, and H. R. Karimi, "Driver state detection for driver-automation shared control with fuzzy logic," *Control Eng. Pract.*, vol. 127, Oct. 2022, Art. no. 105294.
- [25] A.-T. Nguyen, C. Sentouh, and J.-C. Popieul, "Driver-automation cooperative approach for shared steering control under multiple system constraints: Design and experiments," *IEEE Trans. Ind. Electron.*, vol. 64, no. 5, pp. 3819–3830, May 2017.
- [26] A.-T. Nguyen, C. Sentouh, and J.-C. Popieul, "Sensor reduction for driver-automation shared steering control via an adaptive authority allocation strategy," *IEEE/ASME Trans. Mechatronics*, vol. 23, no. 1, pp. 5–16, Feb. 2018.
- [27] J. Han, J. Zhao, B. Zhu, and D. Song, "Adaptive steering torque coupling framework considering conflict resolution for human-machine shared driving," *IEEE Trans. Intell. Transp. Syst.*, vol. 23, no. 8, pp. 10983–10995, Aug. 2022.
- [28] G. Sikander and S. Anwar, "Driver fatigue detection systems: A review," *IEEE Trans. Intell. Transp. Syst.*, vol. 20, no. 6, pp. 2339–2352, Jun. 2019.

- [29] H. Wang et al., "Dynamic reorganization of functional connectivity unmasks fatigue related performance declines in simulated driving," *IEEE Trans. Neural Syst. Rehabil. Eng.*, vol. 28, no. 8, pp. 1790–1799, Aug. 2020.
- [30] A. Nencová et al., "Multimodal features for detection of driver stress and fatigue: Review," *IEEE Trans. Intell. Transp. Syst.*, vol. 22, no. 6, pp. 3214–3233, Jun. 2021.
- [31] T. Huang, R. Fu, Y. Chen, and Q. Sun, "Real-time driver behavior detection based on deep deformable inverted-residual network with an attention mechanism for human-vehicle co-driving system," *IEEE Trans. Veh. Technol.*, vol. 71, no. 12, pp. 12475–12488, Dec. 2022.
- [32] G. Du, T. Li, C. Li, P. X. Liu, and D. Li, "Vision-based fatigue driving recognition method integrating heart rate and facial features," *IEEE Trans. Intell. Transp. Syst.*, vol. 22, no. 5, pp. 3089–3100, May 2021.
- [33] G. Sikander and S. Anwar, "A novel machine vision-based 3D facial action unit identification for fatigue detection," *IEEE Trans. Intell. Transp. Syst.*, vol. 22, no. 5, pp. 2730–2740, May 2021.
- [34] Y. Xing, C. Lv, H. Wang, D. Cao, E. Velenis, and F.-Y. Wang, "Driver activity recognition for intelligent vehicles: A deep learning approach," *IEEE Trans. Veh. Technol.*, vol. 68, no. 6, pp. 5379–5390, Jun. 2019.
- [35] Z. Li, L. Chen, J. Peng, and Y. Wu, "Automatic detection of driver fatigue using driving operation information for transportation safety," *Sensors*, vol. 17, no. 6, p. 1212, May 2017.
- [36] Z. Li, L. Chen, L. Nie, and S. X. Yang, "A novel learning model of driver fatigue features representation for steering wheel angle," *IEEE Trans. Veh. Technol.*, vol. 71, no. 1, pp. 269–281, Jan. 2022.
- [37] Z. Liu, Y. Peng, and W. Hu, "Driver fatigue detection based on deeply-learned facial expression representation," *J. Vis. Commun. Image Represent.*, vol. 71, Aug. 2020, Art. no. 102723.
- [38] A.-T. Nguyen, T. Q. Dinh, T.-M. Guerra, and J. Pan, "Takagi-Sugeno fuzzy unknown input observers to estimate nonlinear dynamics of autonomous ground vehicles: Theory and real-time verification," *IEEE/ASME Trans. Mechatronics*, vol. 26, no. 3, pp. 1328–1338, Jun. 2021.
- [39] H. Zhang, W. Zhao, and J. Wang, "Fault-tolerant control for electric vehicles with independently driven in-wheel motors considering individual driver steering characteristics," *IEEE Trans. Veh. Technol.*, vol. 68, no. 5, pp. 4527–4536, May 2019.
- [40] C. J. Nash and D. J. Cole, "Identification and validation of a driver steering control model incorporating human sensory dynamics," *Vehicle Syst. Dyn.*, vol. 58, no. 4, pp. 495–517, Mar. 2019.
- [41] M. Ahmed, S. Masood, M. Ahmad, and A. A. Abd El-Latif, "Intelligent driver drowsiness detection for traffic safety based on multi CNN deep model and facial subsampling," *IEEE Trans. Intell. Transp. Syst.*, vol. 23, no. 10, pp. 19743–19752, Oct. 2022.
- [42] R. Huang, Y. Wang, Z. Li, Z. Lei, and Y. Xu, "RF-DCM: Multi-granularity deep convolutional model based on feature recalibration and fusion for driver fatigue detection," *IEEE Trans. Intell. Transp. Syst.*, vol. 23, no. 1, pp. 630–640, Jan. 2022.
- [43] K. Mahajan, N. R. Velaga, A. Kumar, A. Choudhary, and P. Choudhary, "Effects of driver work-rest patterns, lifestyle and payment incentives on long-haul truck driver sleepiness," *Transp. Res. F, Traffic Psychol. Behaviour*, vol. 60, pp. 366–382, Jan. 2019.
- [44] A. Craig, Y. Tran, N. Wijesuriya, and H. Nguyen, "Regional brain wave activity changes associated with fatigue," *Psychophysiology*, vol. 49, no. 4, pp. 574–582, Apr. 2012.
- [45] G. N. Dimitrakopoulos et al., "Functional connectivity analysis of mental fatigue reveals different network topological alterations between driving and vigilance tasks," *IEEE Trans. Neural Syst. Rehabil. Eng.*, vol. 26, no. 4, pp. 740–749, Apr. 2018.
- [46] G. Feng, *Analysis and Synthesis of Fuzzy Control Systems: A Model-Based Approach*, vol. 37. Boca Raton, FL, USA: CRC Press, 2018.



Zhenwu Fang (Graduate Student Member, IEEE) received the B.S. degree in mechanical engineering and automation and the M.S. degree in vehicle engineering from the School of Mechanical Engineering, Southeast University, Nanjing, China, in 2017 and 2020, respectively, where he is currently pursuing the Ph.D. degree in vehicle engineering. His research interests include driver-vehicle system dynamics, driver status recognition, and human-machine shared control.



Jinxiang Wang (Member, IEEE) received the B.S. degree in mechanical engineering and automation and the Ph.D. degree in vehicle engineering from Southeast University, Nanjing, China, in 2002 and 2010, respectively. From 2014 to 2015, he was a Visiting Research Scholar with the Department of Mechanical and Aerospace Engineering, The Ohio State University, Columbus, OH, USA. He is currently an Associate Professor with the School of Mechanical Engineering, Southeast University. His research interests include vehicle dynamics and control, assisted-driving systems, and control of autonomous vehicles.



Zejiang Wang received the B.E. degree (Hons.) in mechanical engineering and automation from Southeast University, Nanjing, China, in 2014, the Dipl.-Ing. degree in cyber-physical systems from ENSTA ParisTech, France, the double M.S. degree in design, modeling, and architecture of complex industrial systems from École Polytechnique, University of Paris-Saclay, France, in 2017, and the Ph.D. degree in mechanical engineering from The University of Texas at Austin, Austin, TX, USA, in 2022. His research interests include vehicle dynamics and control, intelligent transportation systems, and human cyber-physical systems.



Jinxin Chen received the B.S. degree in mechanical engineering from the East China University of Science and Technology, Shanghai, China, in 2020, and the M.S. degree from the School of Mechanical Engineering, Southeast University, Nanjing, China, in 2023. He is currently with SAIC Volkswagen Automotive Company Ltd., where he is an Autonomous Driving Algorithm Engineer. His research interests include deep learning, computer vision, and driver-state monitoring systems.



Guodong Yin (Senior Member, IEEE) received the Ph.D. degree in vehicle engineering from Southeast University, Nanjing, China, in 2007. From 2011 to 2012, he was a Visiting Research Scholar with the Department of Mechanical and Aerospace Engineering, The Ohio State University, Columbus, OH, USA. He is currently a Professor with the School of Mechanical Engineering, Southeast University. His current research interests include vehicle dynamics control, connected vehicles, and multiagent control.



Hui Zhang (Senior Member, IEEE) received the B.Sc. degree in mechanical design manufacturing and automation from the Harbin Institute of Technology, Weihai, China, in 2006, the M.Sc. degree in automotive engineering from Jilin University, Changchun, China, in 2008, and the Ph.D. degree in mechanical engineering from the University of Victoria, Victoria, BC, Canada, in 2012. He was a Research Associate with the Department of Mechanical and Aerospace Engineering, The Ohio State University, Columbus, OH, USA. He is the author/coauthor of more than 80 peer-reviewed papers in journals and conference proceedings. His research interests include diesel engine aftertreatment systems, vehicle dynamics and control, mechatronics, robust control and filtering, networked control systems, and signal processing.